

# Understanding the Free Energy Landscape of Phase Separation in Lipid Bilayers using Molecular Dynamics

Ashlin J. Poruthoor<sup>1</sup> and Alan Grossfield<sup>1,\*</sup>

<sup>1</sup>University of Rochester Medical Center, Rochester, NY 14620

\*Correspondence: alan\_grossfield@urmc.rochester.edu

## ABSTRACT

Liquid-liquid phase separation (LLPS) inside the cell often results in biological condensates that can critically impact cell homeostasis. Such phase separation events occur all across a cell and often involve common biomolecules, including lipids in the cell membranes. Lipid phase separation at the cell membrane and subsequent ordered domain formation in a sea of disordered lipids led to the so-called "lipid raft hypothesis." The resulting lipid domains often have functional roles. However, the thermodynamics of lipid phase separation and their resulting mechanistic effects on cell function and dysfunction are poorly understood. Understanding such bulk phenomenon on a cell membrane with a diverse lipidome is exceptionally difficult. Hence simple model systems that can recapitulate similar behavior are widely used to study this phenomenon. Despite simplifying the problem, the relative timescale and system size required for simulating phase separation events pose a challenge for molecular dynamics (MD) simulations. Thus, most MD studies focus on spontaneous lipid phase separation as an adequate sampling of transition events between mixed and separated lipid states is hard to achieve by the current MD framework. Here, we propose a proof-of-concept pipeline that can realize such multiple-state transitions by combining coarse-grained model membranes with enhanced sampling protocols. Using this pipeline, we can ask not just whether a system phase is separated or not, but why it separates, with statistical rigor.

## INTRODUCTION

Interactions among biomolecules often result in phase separation and subsequent formation of biological condensates(1). In the past decade, there has been a new appreciation for the role of phase separation in cell physiology(2). Biological condensates involving fundamental biomolecules like DNA(3), RNA(4), protein(5), and lipids(6) are identified, and their functional roles are characterized. Biological condensates have been observed to be involved in diverse processes, including DNA damage response(7), translational(8) and transcriptional(9) regulation, ribosome biogenesis(10), cell adhesion(11), and endocytosis(12). Such nano-to-micron-scale compartments have no surrounding membrane but sequester key molecules and help in cellular organization, similar to canonical organelles(13, 14). These transient and dynamic sequestration zones are crucial for cell stress responses(14) and signal transductions(15). As phase-separated molecules are concentrated within these condensates, they can function as reaction crucibles that enhance reaction kinetics(16). However, abnormal phase behavior of biological condensates is speculated to underlie multiple disease states, including neurodegenerative diseases such as Huntington's(17), ALS(18), and Parkinson's(19).

Like the intracellular biological condensates, phase separation in the cell membrane often results in relatively ordered lipid lateral domains with collective behavior that can recruit other proteins and lipids(6, 20). Such domains often cluster signaling molecules(21) and facilitate conformational modulations through domain-specific lipid interactions(22, 23) that are relevant in immune signaling(24),(25) and host-pathogen interactions(26). As membrane properties modulate resident protein function, the coexistence of distinct phases gives the cell extra grip on regulation. Conformational changes in domain resident molecules and their subsequent activity shift regulates key signaling events(22, 23). It has also been observed that the HIV Gag protein is sensitive to domains with high cholesterol content, suggesting a potential role of membrane domains in host-pathogen interaction and viral assembly(26). Moreover, lipid domains are conserved throughout the tree of life, implying its relevance in regulating cellular processes(6). Thus, calculating the thermodynamics of phase separation as a function of the composition of the system is critical in understanding the molecular grammar behind lipid domains and the resultant functional modulations.

Lipid domains have been studied from the perspective of phase separation experimentally and computationally. However, teasing out the complex interactions between domain components that determine the membrane organization is challenging in vivo due to the limitations of different methodologies(27). Such difficulties primarily arise due to (a) the complex composition

of cell membrane(28), (b) difficulties in defining domain properties *in vivo*(6), and (c) challenges in achieving specificity when perturbing the system with probes(29). Hence simple model membranes have been extensively used to mimic the phase separation of complex cell membrane phenomenon *in vitro*(30–32) and *in silico*(33–35). Such studies provide powerful insights into phase-separated domains, their properties, and whether the process is favorable, but they often fail to quantify the underlying thermodynamics. Similarly, the resulting mechanistic effects on cell function and dysfunction due to lipid phase separation need to be better understood.

As a "computational microscope"(36)," molecular dynamics (MD) simulations have been used to study spontaneous lipid separating without using exogenous labels or probes(37). However, MD simulations designed for spontaneous phase separation are inadequate to compute thermodynamic properties with statistical confidence. This is because the transition between mixed and separated system-states is often a single irreversible event on the microsecond timescale typically achievable by typical all-atom MD. Additionally, the relatively large size required to model this bulk phenomenon significantly increases computational costs. To circumvent this limitation, coarse-grained (CG) MD simulations have been used to study spontaneous phase separations in model membranes(33, 38). CG-MD is an ideal tool to study phase separation in the membrane due to its inherent advantage of high spatial and temporal resolution while capturing nanoscale domains due to transient phase separation events. Previously, the Tieleman(38) and the Gorfé groups(35) have done some pioneering work on the thermodynamics of lipid domains. While the former used thermodynamic integration(39) to calculate the free energy and excess chemical potential for exchanging lipid species between phases, the latter used umbrella sampling(40) to compute the membrane partition thermodynamics of an idealized transmembrane domain by dragging it across distinct lipid phases.

We hypothesize that coupling a more versatile enhanced sampling method with the standard CG-MD will improve the transition events between the mixed and separated states of the lipid bilayer system under study to compute the free energy for phase separation. Various enhanced sampling protocols have previously demonstrated their ability to enhance the sampling of rare events(41). In most cases, external forces are applied to the system to bias simulation to explore the desired phase space. Generally, it is necessary to compute the collective variable or its derivative at each time step as the dynamics proceeds. Certain popular implementations of such protocols, like COLVARS(42) and PLUMED(43), are done on single CPUs serially, leading to poor performance when the collective variable is computationally complex, as is the case for phase separation. This often involves determining the centroid of each lipid and the subsequent all-to-all distance determination within each leaflet. Thus complex CV calculation at every time step of the MD is not desired.

However, weighted ensemble (WE)(44) has the advantages of (a) unbiased dynamics, and (b) good sampling by enhancing the sampling of otherwise undersampled phase space and reducing the sampling of otherwise oversampled phase space; therefore, judiciously using the given computational resources(44). Moreover, there is an added benefit that the calculation of the collective variable can be decoupled from the MD, which simplifies the implementation and improve the computational performance. As the collective variable can take complex functional forms in our case, it reduces extra computational costs. It should be noted that the WE method is highly parallelizable and can take advantage of GPU acceleration(45). Hence we decided to use the WE strategy to enhance the sampling of transition from mixed to separated and vice versa in CG-MD simulation.

Here we present a novel proof-of-concept pipeline to realize multiple mixing and separating events in a lipid bilayer system and state the equilibrium free energy. Thus a quantitative thermodynamic description of the system can be made using this tool to know how the fine-tuning of its composition results in distinct lipid domains that can coexist with functional differences but shared components. We test this pipeline on three different lipid bilayer systems with varying degrees of phase separation propensity. We discuss one well-known pitfall of enhanced sampling techniques that we encountered - identifying a good collective variable. We explore three potential candidates for collective variables and assess their effectiveness in the pipeline. We then construct free energy landscapes of the three systems at multiple temperatures. We further explore a few non-traditional use cases for the data thus generated and discuss additional room for improvements.

## METHODS

### System details

As shown in Fig 1, we used three different ternary lipid bilayer systems: 1. A lipid bilayer consisting of dipalmitoyl-phosphatidylcholine (DPPC), dilinoleyl-phosphatidylcholine (DIPC), and cholesterol (CHOL), known to phase separate *in silico* in a few microseconds (15, 33, 46–50). 2. A lipid bilayer consisting of DPPC, diarachidonoyl-phosphatidylcholine (DAPC), and CHOL, known to phase separate *in silico* within a few hundred nanoseconds (34, 35, 51). 3. A lipid bilayer consisting of DPPC, palmitoyl-oleoyl-phosphatidylcholine (POPC), and CHOL that was previously shown not to phase separate (32, 51). The composition of DPPC-DIPC-CHOL, DPPC-DAPC-CHOL, and DPPC-POPC-CHOL systems used here are (0.42/0.28/0.3), (0.5/0.3/0.2) and (0.4/0.4/0.2) respectively and are adapted from previous studies (33, 34, 51). Similar to the previous studies, we kept the total number of lipids in DPPC-DIPC-CHOL, DPPC-DAPC-CHOL, and DPPC-POPC-CHOL at 1944, 1200 and 1200

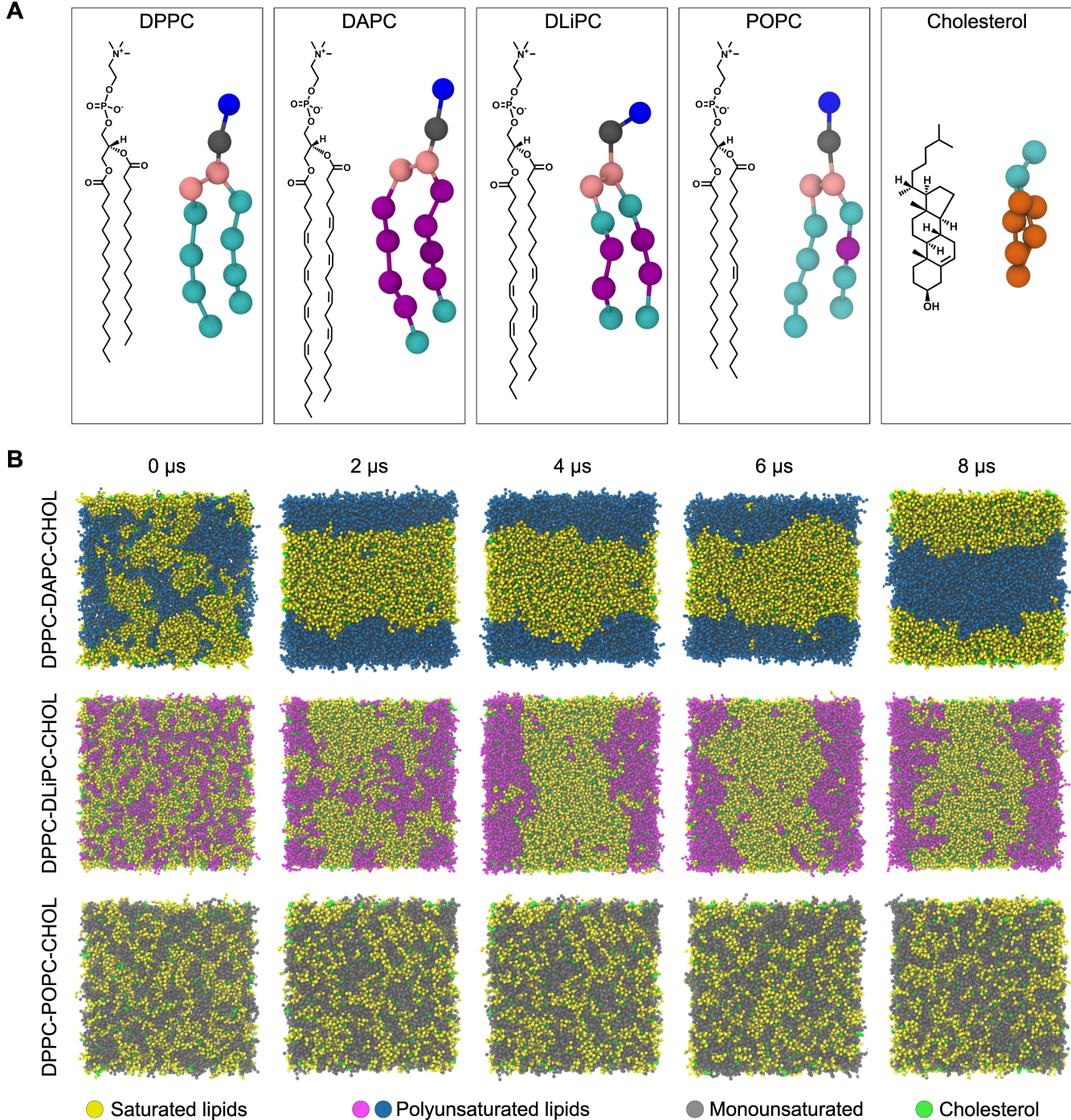


Figure 1: A. 2D structure and corresponding MARTINI 2 bead structure for lipids used in this study. B. Time evolution of each lipid system as a function of time. The membrane normal is pointing towards the reader

respectively.

Due to the relatively large system sizes and the time scale required for phase separation and related dynamics in lipid bilayer simulations, we used the coarse-grained (CG) model for each system. Hence the subsequent dynamics propagation using MD is relatively cheaper than an all-atom model but with a tradeoff in system resolution. The rationale behind this design choice is to fail faster with minimum resources if this proof-of-concept protocol is not working as expected. Using CHARMM-GUI Martini Maker (52), we constructed four random replicas of each CG ternary symmetric bilayer system. We used MARTINI 2 force

field parameters and particle definitions<sup>(53, 54)</sup> to construct CG systems and to run the subsequent MD simulation. We replaced the default input files from CHARMM-GUI Martini Maker with their respective most recent Martini 2.x versions if they existed. We used MARTINI polarizable water model<sup>(55)</sup> to solvate all systems with approximately a 1:30 lipid to real water ratio. A detailed description of the systems is given in Table S1 of supplementary material. We did not use the more recent MARTINI 3.0 lipid parameters since there were no published MARTINI 3 parameters for cholesterol at the time of the writing.

## Standard MD simulation details

Due to the historical compatibility of the GROMACS MD engine with the MARTINI force field, we used GROMACS 2020.3<sup>(56)</sup> to propagate the dynamics of the systems prepared. Each system was minimized and equilibrated in steps using the MD input files suggested by CHARMM-GUI Martini Maker. To obtain an intact bilayer without any membrane undulations, we used an additional membrane restraining protocol: We took advantage of the flat bottom restrain potential available in GROMACS to allow lipids to move freely in the *xy* plane but restrained within a slab of defined *z* thickness. More details about membrane restraining protocol are given in the supplementary material.

After the minimization and equilibration, all systems were run at 400 K in the NPT ensemble for 100 ns to make sure the lipids in each system were randomly distributed. For every system, we forked each replica into multiple temperature runs simulated at different temperatures ranging from 298K to 450K. For these production runs, the temperature coupling is done using velocity rescaling<sup>(57)</sup> with a time constant 1 ps. An extended-ensemble Parrinello-Rahman pressure coupling<sup>(58)</sup> with a relatively high time constant of 12 ps was used as we are dealing with CG system. A semiisotropic pressure coupling suited for membrane simulations is used here with a compressibility of  $3e^{-4}$  bar<sup>-1</sup> and reference pressure for coupling as 1 bar. A reaction field electrostatics with Coulomb cutoff of 1.1 nm was used. Since we are using a polarizable water, a relative dielectric constant of 2.5 was used. For Van der Waals interaction, a similar cutoff of 1.1 nm was used. A potential-shift Van der Waal modifier was also used. For neighbor searching, a verlet cutoff scheme was used with neighbor list updated every 20 steps. The simulation parameters were mostly inspired by previous CG MARTINI simulations<sup>(59)</sup>. To eliminate potential artifacts previously reported<sup>(60)</sup>, for LINCSolver<sup>(61)</sup>, we used 8 as the highest order in the expansion of constraint coupling matrix for more accuracy. Moreover, for better energy conservation, we also used short 20 fs timesteps, which is conservative for a CG system.

All standard MD simulations ran for at least 8 microseconds using the BlueHive supercomputing cluster of the Center for Integrated Research and Computing at the University of Rochester. Simulations ran on Intel Xeon E5-2695 and Gold 6130 processors augmented with Tesla K20Xm, K80, and V100 GPUs. The trajectories were processed and analyzed using the LOOS software package. A detailed description of the simulation parameters is given in Table S1 of supplementary material.

## Collective Variable

A collective variable (or a set of variables) is a reduced coordinate that captures the progress of a system along the transition of interest. Ideally, such a reduced variable(s) should fully capture the key modes of the system to reflect the complex event under study. The success of any enhanced sampling protocol depends on the chosen collective variable over which the sampling is enhanced<sup>(41, 62, 63)</sup>. Thus to drive the WE simulation, we used three candidates for the collective variable.

### 1. Fraction of Lipids in Cluster (FLC)

Since the formation of lipid domains with distinct properties from the rest of the bilayer is a characteristic feature of a phase-separating lipid bilayer, we hypothesized that we could use a variable that quantifies the recruitment of lipids into such domains to track the phase separation events in our systems. Here, we define the Fraction of Lipids in Cluster (FLC) as follows:

$$\text{FLC} = \sum_i^N \frac{\text{No. of } X_i \text{ lipids in lipid } X_i \text{ Clusters}}{\text{No. of Lipid } X_i} = \frac{\sum_i^N \text{No. of Lipid } X_i \text{ in Lipid } X_i \text{ Clusters}}{\text{Total No. of Lipids}} \quad (1)$$

Where subscript *i* denotes the individual lipid species in a bilayer consisting of *N* total lipid species. As shown in Figure 2, each system under study has *N* = 3 lipid species. FLC increases as the system goes from a mixed state, with a random distribution of lipids, to a separated state. In principle, the bounds of FLC are between 0 and 1. FLC = 0 corresponds to a system configuration where no lipids are part of any cluster. While FLC = 1 corresponds to all lipids being a part of some cluster.

The lipid *X<sub>i</sub>* cluster is defined using the Density-Based Spatial Clustering of Applications with Noise (DBSCAN) algorithm<sup>(64, 65)</sup> as implemented in scikit-learn<sup>(66)</sup>. For lipid DBSCAN clustering, instead of the default euclidean metric to calculate the distance between lipid coordinates, we used a precomputed distance matrix adjusted for periodic boundary conditions of the simulation box using LOOS<sup>(67)</sup>. The algorithm requires two additional input parameters: *min\_samples* and *ε*. We consider

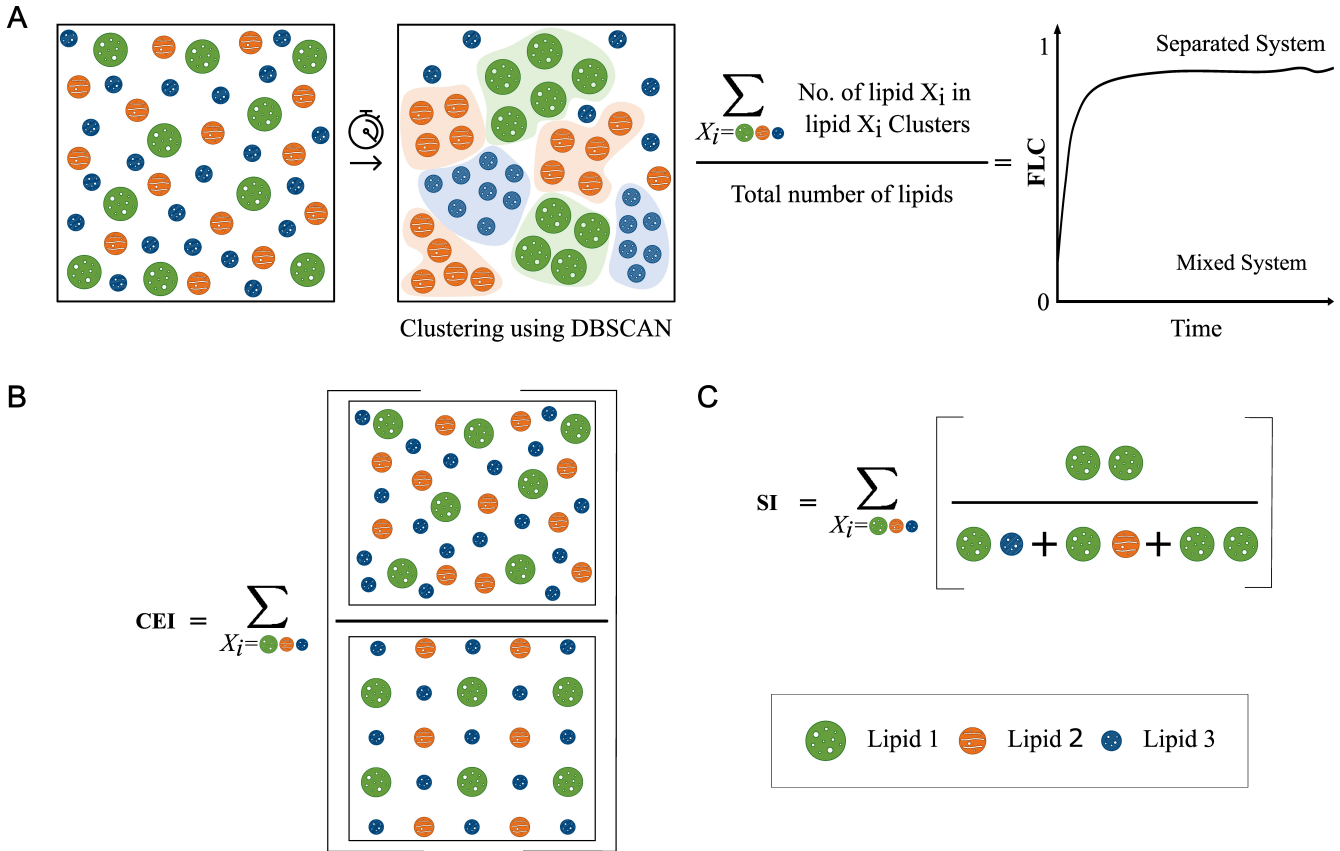


Figure 2: A. Illustration of FLC : Functional form of FLC and expected evolution curve for a phase separating system. B. Illustration of Cummulative Enrichment Index. C. Illustration of Seggregation Index

lipids with more than  $\text{min\_samples}$  neighbors (including the lipid itself) within  $\epsilon$  radius as core lipids. Non-core lipids still within  $\epsilon$  radius of a core lipid are considered border lipids. A set of core lipids within  $\epsilon$  radius of each other and their border lipids forms a cluster. All lipids that are not a part of any cluster are considered outliers.

Since lipid motion in a bilayer is constrained primarily on a plane and MARTINI beads for a lipid are of similar radii, we can use the two-dimensional version of Kepler's conjecture that the densest packing of unit disks in a plane is hexagonal close packing (Thue's Theorem). Hence we chose 7 (6 nearest neighbors + 1 central lipid) as  $\text{min\_samples}$  for all the lipid species. However,  $\epsilon$  was chosen differently for each lipid species based on their first nearest neighbor distance from the central lipid. We used the *xy\_rdf* tool in LOOS to calculate an individual lipid species' first nearest neighbor distance. From the first 8  $\mu\text{s}$  MD standard simulation of each replica, we computed the radial distribution function (RDF) for a lipid species in the xy-plane. From the RDF plot, we found the first maxima (provided it is above 1), and the distance to the minima right after this first maximum was determined to be the first nearest neighbor distance for that lipid species. This distance was averaged over all four replicas for a given system at a given temperature and then assigned as the respective  $\epsilon$  input. Since nearest neighbor distance is a function of temperature, for the same lipid species in the same system,  $\epsilon$  may be different for different temperatures. Computed  $\epsilon$ , i.e., average first nearest neighbor distance for different conditions, are plotted in Supplementary Figure S1. Additionally, we tracked auxiliary variables (AVs) that evaluate the quality of DBSCAN clustering since it is critical for defining the FLC that drives the WE equilibrium dynamics.

## 2. Cumulative Enrichment Index (CEI)

We defined a density-based quantity to estimate the degree of global lipid enrichment in the system, similar to the ones that track local lipid segregation used previously (68, 69). Here, we calculated the average local density of  $X_i$  lipids around a single lipid  $X_{ij}$ , within a cutoff radius,  $\epsilon_i$ , as we defined earlier for FLC estimation. The cutoff radius,  $\epsilon_i$ , is also temperature dependent. We also defined a normalization factor,  $\Phi_i$ , as the local density of  $X_i$  lipids for a uniformly well-mixed system of similar composition. The ratio of former respective to latter forms the enrichment index for a lipid species,  $X_i$ . CEI is defined as the

sum of individual enrichment index for all the lipid species in the system, as follows:

$$\begin{aligned} \text{CEI} &= \sum_i^N \left[ \frac{\text{Average local density of lipids } X_i \text{ around a single lipid } X_i}{\text{Local density of lipid } X_i \text{ for a well mixed system}} \right]_{\epsilon_i(T)} \\ &= \sum_i^N \frac{1}{\Phi_i} \frac{1}{\pi \epsilon_i^2} \sum_j \text{No. of } X_i \text{ lipids around } X_{ij} \text{ lipid in } \epsilon_i(T) \text{ radius} \end{aligned} \quad (2)$$

Where  $X_{ij}$  denotes  $j^{th}$  lipid of  $X_i$  lipid species. The local density around  $X_{ij}$  is calculated within  $\epsilon_i(T)$  distance, where T is the temperature of the system. We correct the local density for central lipid contributions. For the normalization factor,  $\Phi_i$ , we calculated the global density of  $X_i$  lipids by taking the ratio of the total number of  $X_i$  lipids in the system to the  $xy$ -planar area of the bilayer system. This global density is the same as the local density of  $X_i$  lipid for a uniformly well-mixed system. Thus CEI significantly larger than 3 implies that the ternary system,  $N = 3$ , deviates from a well-mixed state to a separated state.

### 3. Segregation Index (SI)

We defined a contact-based quantity to track the homogeneity of the lipid bilayer, similar to the ones that track the mixing of beads used previously(70, 71). Here, we calculated the fraction of like contacts made between  $X_i$  species to the total contacts made by  $X_i$  as shown below:

$$\text{SI} = \sum_i^N \left[ \frac{X_i X_i}{\sum_j^N X_i X_j} \right]_{\epsilon_i(T)} = \frac{X_{11}}{X_{11} + X_{12} + X_{13}} + \frac{X_{22}}{X_{21} + X_{22} + X_{23}} + \frac{X_{33}}{X_{31} + X_{32} + X_{33}} \quad (3)$$

$X_i X_j$  denotes the contacts between lipid species  $X_i$  and  $X_j$  within  $\epsilon_i(T)$  cutoff. Thus for a ternary bilayer system,  $\text{SI} = 3$  implies a fully separated system, and  $\text{SI} < 3$  implies mixing. However, for the analysis, we ignored the contribution of cholesterol as we found that excluding the cholesterol term did not change the functional behavior (Supplementary Info). Hence,  $\text{SI}_{\text{noCHOL}}$  effectively will have bounds [0, 2] unless otherwise stated.

## Weighted Ensemble Simulation

### Preparing seeding configurations for WE simulation

From each 8  $\mu$ s replica MD simulation of a given system, the last ten frames spaced by 100 ns were collected. Using such collected frames, we created sets of mixed and separated configurations for each system replica. For DPPC-DAPC-CHOL and DPPC-DIPC-CHOL systems, the set of mixed configurations for a particular replica came from the respective 423 K and 450 K simulation frames. The set of separated configurations for a replica comes from the respective 298K and 323K simulation frames. For the DPPC-POPC-CHOL system, sets of mixed and separated configurations for a replica came from the 450 K and 298K simulation frames, respectively. To enhance the convergence of WE equilibrium simulations, we decided to seed each simulation from mixed and separated states and let the enhanced sampling cover the transition between them.

### Running WE simulations

We ran weighted ensemble equilibrium simulations using the WESTPA 1.0 software package(45) closely following the previously established protocol(72). The collective variable was divided into 30 dynamic bins using the minimal adaptive binning scheme (MAB)(73). For each replica, a target number of 4 short simulations, or "walkers" per bin, were started in parallel from the mixed and the separated configurations prepared earlier. After every resampling interval of 1 ns, the collective variable was evaluated to initiate the merging and splitting of walkers to maintain the target number of walkers per bin. A short one ns MD run of all the walkers and subsequent resampling, according to the standard WE algorithm, constituted 1 WE iteration. We conducted 500 WE iterations for each replica. We used GROMACS 2020.3 engine to propagate with the same parameters used for standard MD simulations described earlier. The WE Equilibrium Dynamics (WEED) reweighting protocol(74, 75), implemented in WESTPA 1.0, was used to accelerate the convergence of WE walkers toward equilibrium. The reweighting is done every 10 WE iterations. Four independent WE replicas were simulated each temperature for each lipid composition. All WE simulations ran using the Intel Xeon E5-2695 and Tesla K20Xm GPUs in the BlueHive supercomputing cluster of the Center for Integrated Research and Computing at the University of Rochester.

## Analysis of WE simulations

The probability distributions for the CVs for each replica, as a function of WE iterations, was constructed using *w\_pdist* and *plothist* tools in WESTPA. Using this distribution, we monitored the evolution of each WE replica simulation and the convergence. We used the *w\_multi\_west* tool in WESTPA to combine data from four WE replicas of a system at a given temperature. We then constructed the respective free energy surface from the combined probability distribution of a system. To check populations in different states and the flux between states the *w\_ipa* tool was used.

## RESULTS

Consistent with previous studies from which they are adapted, the standard CG MD simulations of DPPC-(DA/DI)PC-CHOL systems phase separates into L<sub>o</sub> and L<sub>d</sub> regions. The L<sub>o</sub> region is enriched in saturated lipid, DPPC, and cholesterol. The L<sub>d</sub> region is enriched with unsaturated lipids (DA/DI)PC. The DPPC-POPC-CHOL system showed low to no separation. This section compares how different variables track phase separation propensity in lipid bilayers using standard CG MD simulations. We then compare the convergence of WE simulation to the choice of collective variable. Finally, we present the free energy landscapes of lipid bilayer systems obtained using WE simulations and discuss reusing the data generated to form other intuitions and applications.

To evaluate how collective variables, FLC, and other auxiliary variables track phase separation in lipid bilayers, from standard CG MD, we traced the time evolution of each variable for different systems at different temperatures. Figure 3 illustrates the temporal evolution of FLC, CEI, and SI<sub>noCHOL</sub> for DPPC-(DA/DI/PO)PC-CHOL systems at 298K, 323K, 423K, and 450K. For DPPC-(DA/DI)PC-CHOL systems, the variables capture a single transition between a mixed state and a separated state. Also, the systems reside dominantly in a separate state after the transition in the standard CG simulation. Interestingly, for relatively slow separating DPPC-DIPC-CHOL, CEI and SI<sub>noCHOL</sub> tracks a relatively slower state transition than FLC. However, for the DPPC-POPC-CHOL system, the variables capture a single state corresponding to a mixed system and no transition. Nevertheless, it is worth noting that FLC, CEI, and SI<sub>noCHOL</sub> capture the effect of temperature in all systems, including the negative control that does not phase separate. These variables even capture the subtle differences in phase-separating propensity between systems. For example, at 298K, the plateaued region of the FLC, CEI, and SI<sub>noCHOL</sub> curves are higher for the DPPC-DAPC-CHOL system than the DPPC-DIPC-CHOL system. This is expected as (a) the lipid chain mismatch between saturated and unsaturated lipid species and (b) the number of double bonds in unsaturated lipid species is more in the DPPC-DAPC-CHOL than DPPC-DIPC-CHOL system. Both these factors have previously been shown to influence lipid phase separation kinetics and domain stability(34, 76). Thus we have a set of low-dimensional variables that can (a) represent the global dynamics of the lipid bilayer system, (b) distinguish and track the transition between mixed and separated states, (c) capture the temperature effects, and (d) based on the composition of the system. The time evolution of other auxiliary variables can be found in Fig SX.

## Choice of collective variables for WE simulations

Since the density based, CEI, contact-based SI<sub>noCHOL</sub> and clustering based FLC tracks bilayer lipid separation similarly, we decided to use them as progress coordinates to drive the WE simulation. However, the free energy landscapes generated using these variables, after running 500 WE iterations, give conflicting results for the same system. As shown in Fig 4A, for the test system DPPC-DIPC-CHOL replica at 323K, the free energy landscape do not agree with each other despite the number of WE iterations used to construct them being identical. From CEI free energy landscape, we see both states are equally likely. SI<sub>noCHOL</sub> landscape suggests a mixed state is more likely than a separated state. However, both these results deviate from what we observe with standard CG MD simulation, where the DPPC-DIPC-CHOL system slowly separates into L<sub>d</sub> and L<sub>o</sub> regions and stay separated for the most of simulation. Moreover, disagreement of free energy curves as a function of WE iteration blocks used to generate them suggests that the underlying sampling needs to converge more. On the other hand, FLC free energy landscape shows that the separated state is favorable, but the free energy barrier between the two states is small. Additionally, there is a convergence between FLC free energy curves as we proceed with WE iterations. Thus, all three free energy landscapes show a double well, identifying two states but disagreeing on the state the system is most likely to be in and the relative free energy difference between states. Interestingly, if we monitor the evolution of configurational distributions of each variable as a function of WE iterations, all three show a converged behavior, as shown in Fig 4B.

These conflicting results raise the following questions: Why do variables that make perfect sense while tracking the system in standard CG MD simulation gives a different free energy landscape after WE simulation? Why do CEI and SI<sub>noCHOL</sub> that show converged configurational distributions as a function of WE iterations, does not give converged free energy curves with each other as WE proceed?

The configurational distribution of collective variables staying mostly undisturbed in two states (Fig 4B) and the free energy

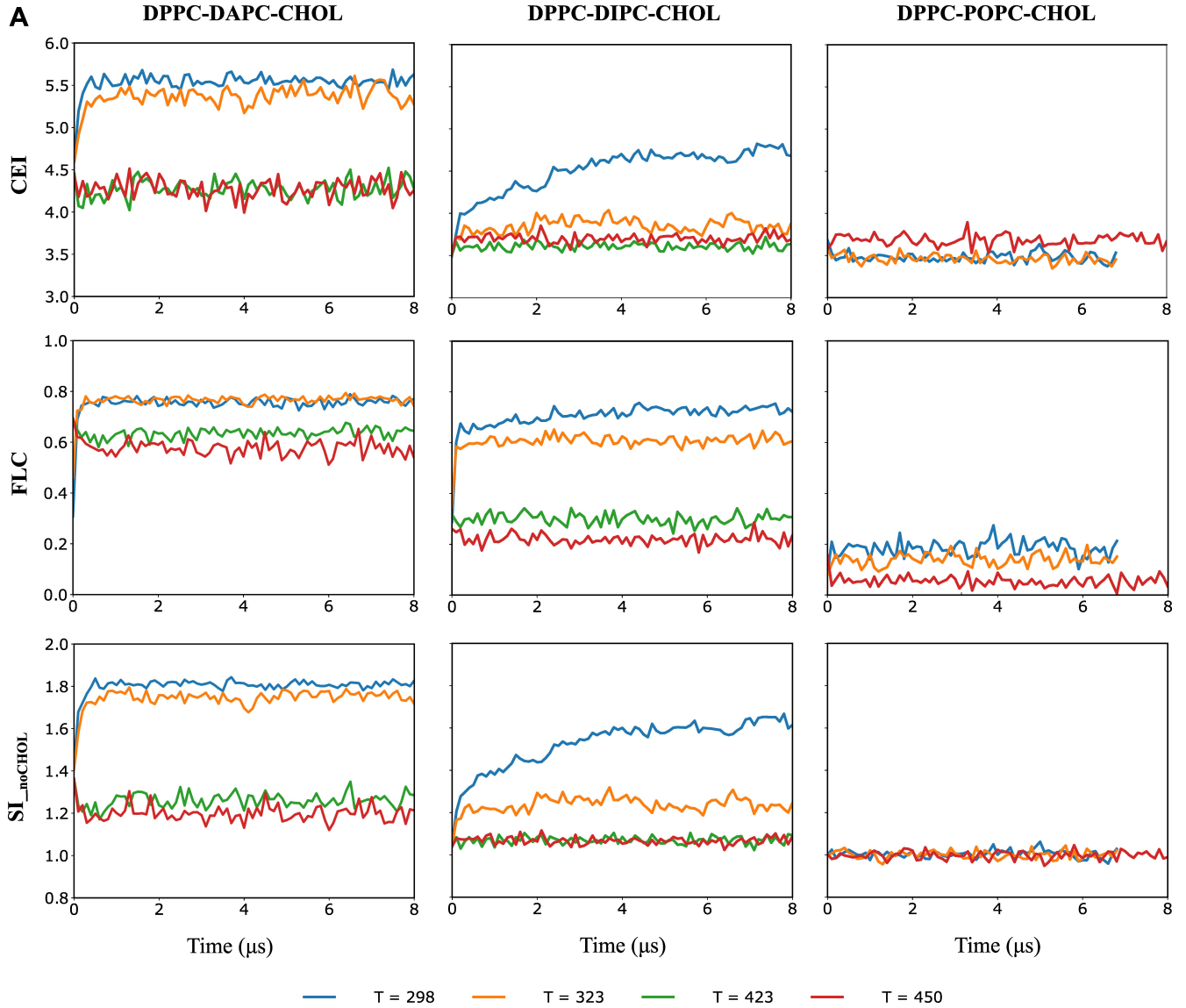


Figure 3: A. Time series for three collective variables tracking membrane separation. Each line represents a conventional MD simulation started from a well-mixed state. Each column contains trajectories from a single lipid composition, while each row shows a different variable; 8 $\mu$ s trajectories were used for all rows. The lines are colored to represent different simulation temperatures.

curves struggling to converge on the state basins and free energy barrier for CEI and SI<sub>noCHOL</sub> landscapes (Fig 4C) suggest that there might not be adequate state crossing of walkers populating each state. Hence we decided to check the flow rate of probability across the states. To calculate the flux between states, we need to define the states for each collective variable. We define mixed and separated states as CEI = [0.0, 3.9] and [4.4, 6.0], SI<sub>noCHOL</sub> = [0.0, 1.3] and [1.4, 2.0], and FLC = [0.0, 0.575] and [0.65, 1.0] respectively. Please note that the state bounds are chosen based on visual inspection of the corresponding free energy landscapes in Fig 4A. The choice is arbitrary but ad hoc enough to give us a picture of what is happening. Fig 4C shows the mean flux from mixed to separated state and vice versa in WE simulation driven using each collective variable. Here, mean flux is calculated for a window of 10 WE iterations as the WEED reweighting protocol is done every ten iterations to accelerate the convergence. The peaks in these plots imply probability crossing states. For CEI, no state crossing occurs between mixed to separated, and vice versa during WE simulation. For SI<sub>noCHOL</sub>, the state crossing back and forth is practically zero during the first few hundreds of WE iterations. Meanwhile, for FLC, flux into and out of the states is relatively higher and more immediate than the other two variables. These results are supported by the corresponding state population evolution as a function of WE

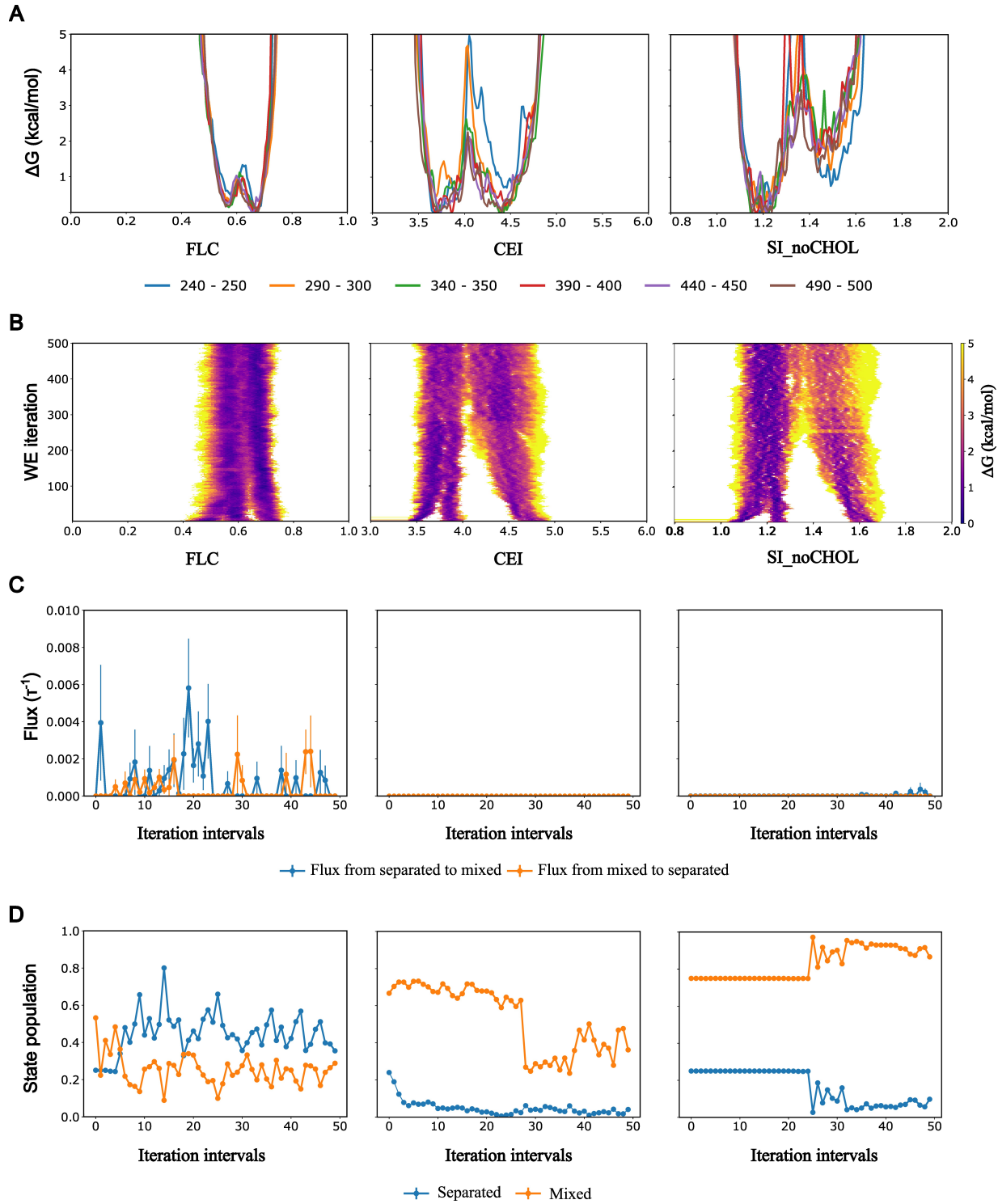


Figure 4: For the given DPPC-DIPC-CHOL replica: A. Free energy curves as a function of WE iteration blocks used to generate them. B. Each plot gives the evolution of configurational distribution for a given collective variable. C. Flux profile between states. The peaks represent crossing of walkers. D. Corresponding state population. Here, each column represent the collective variable that was used to drive WE simulation (FLC, CEI, and SI<sub>noCHOL</sub>).

iterations, as shown in Fig 4D. Here, the normalized walker population occupying a specific state is calculated for 10 WE iterations, similar to Fig 4C.

The walkers crossing bins and thereby constituting a flow of probability between states is crucial for the success of a WE equilibrium simulation(44). Thus these results suggest that for CEI and  $SI_{noCHOL}$  variables, the initial distribution of walkers is not disturbed throughout the WE simulation. Without sufficient state crossing, the initial configurational distribution is not relaxing into a well-sampled equilibrium distribution for WE simulations driven by CEI and  $SI_{noCHOL}$  even after 500 iterations. This explains why in free energy landscapes associated with CEI and  $SI_{noCHOL}$ , we do not see converged free energy curves as WE proceed. However, as WE proceed, we see good state crossing and relatively well-converged free energy curves for FLC. The combined results from standard CG MD and WE simulations suggest that CEI and  $SI_{noCHOL}$  are suitable proxy labels for phase separation. However, a poor choice for a collective variable to drive WE simulations. We also found that free energy curves generated by FLC-driven WE simulation are consistent across replicates (Fig SX). Hence we decided to go forward with FLC-based WE simulation to enhance the sampling of phase separation events in lipid bilayer systems to understand the underlying thermodynamics.

## Free energy landscapes of lipid bilayer systems

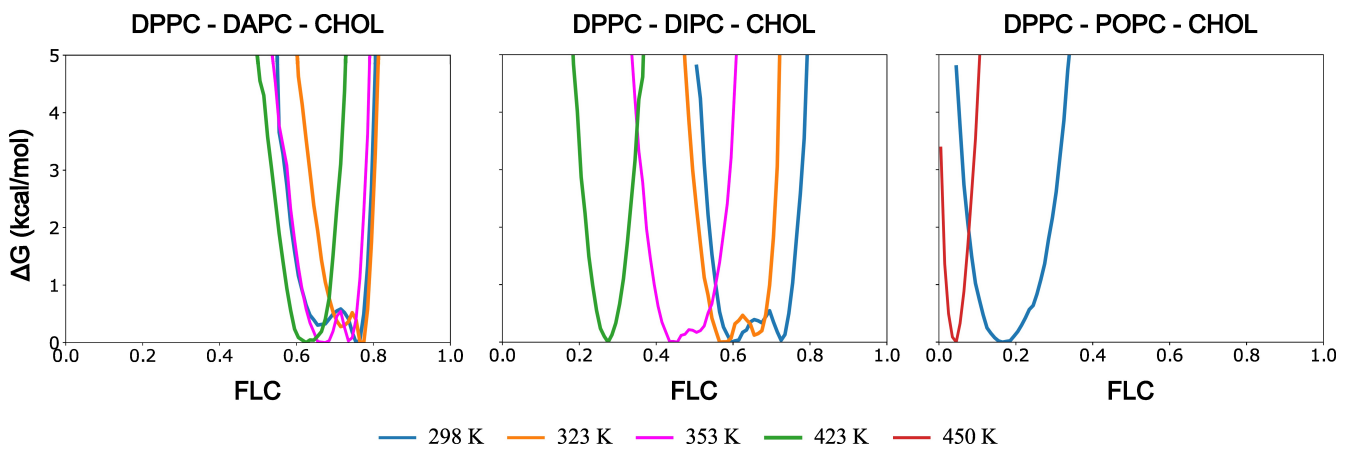


Figure 5: Free energy landscape based on FLC driven WE simulation for three systems. Each line represents a free energy curve. Each column contains free energy curves from a single lipid composition. The lines are colored to represent different simulation temperatures

Figure 5 shows the free energy profiles of DPPC-DAPC-CHOL, DPPC-DIPC-CHOL, and DPPC-POPC-CHOL lipid bilayer systems. Each curve is generated by averaging four WE replica simulations, as mentioned in the Methods section. Individual replica contribution is obtained by averaging the last ten iterations of the respective replica WE simulation (491-500). The positive control, DPPC-DAPC-CHOL system that readily phase-separates, has a double well behavior at 323K and 353K. However, both basins correspond to relatively high FLC. In addition to the free energy curve at 423 K, we see that regardless of high temperature, this system prefers to be in configurations where more than 60% of lipids are in some clusters. For the negative control, DPPC-POPC-CHOL system, the free energy curves at 298K and 423K have single basin nature and correspond to a low fraction of lipids preferring to be in any clusters. For the test system, DPPC-DIPC-CHOL system, as the temperature increases, the characteristic double-well transition to single-well curves, and the width of free energy curves decreases. In general, FLC-based free energy landscapes capture the role of lipid species constituting the bilayer system in its phase separation. Moreover, the effect of temperature in decreasing the propensity of a lipid bilayer to separate is evident in all systems. Please note that though the expectation of clustering-based FLC is to track the formation of domains in a lipid bilayer, the fact that it also neatly captures the temperature effect, even for the negative control, suggests the robustness of FLC as the collective variable.

## Reconstructing free energy landscapes

One outcome of WE simulation is the curated ensemble of diverse trajectories/walkers. By construction, WE resampling ensures that the weights associated with these walkers are unbiased. Thus, we can reuse these weights to examine other variables of choice post-simulation. Assuming the initial configurational distribution relaxed into an equilibrium distribution during WE simulation driven by FLC (see Discussion), by reusing the weights, we have reconstructed analogous free energy

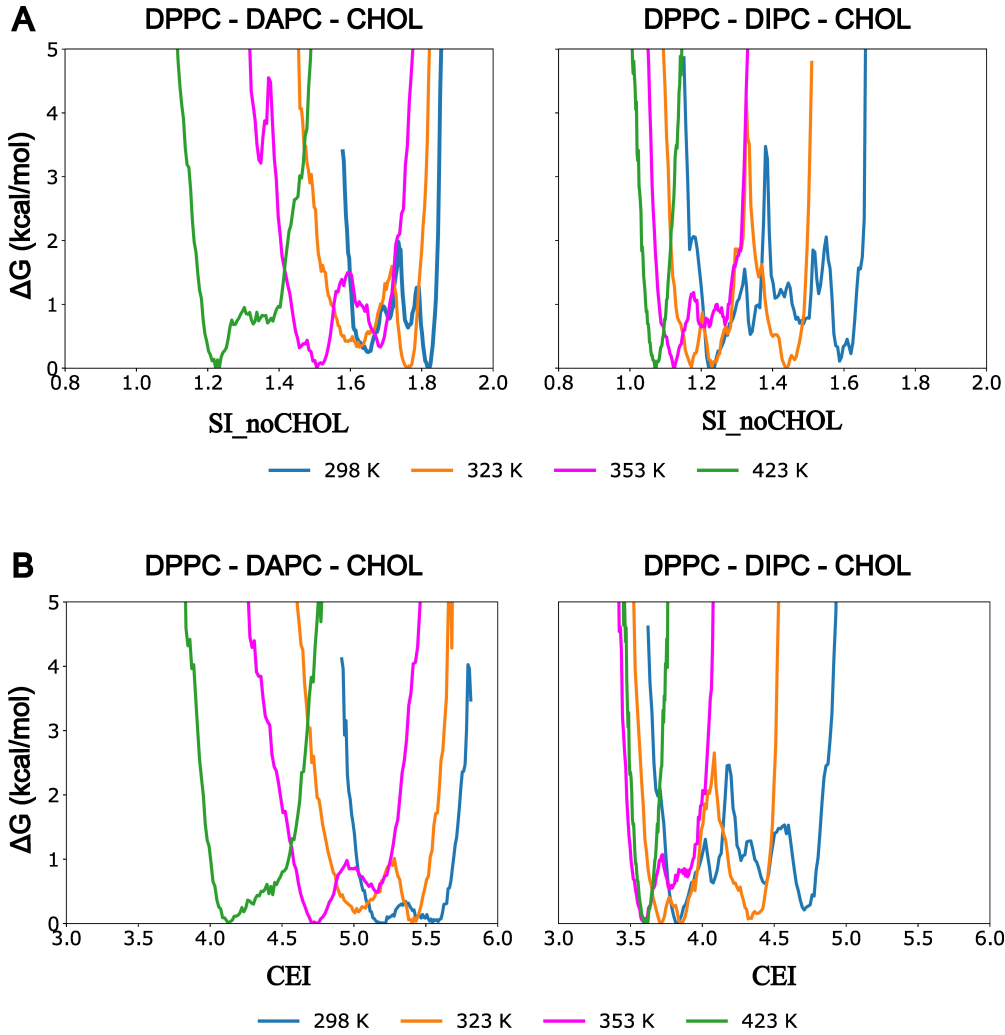


Figure 6: A. Free energy landscapes reconstructed using the ensemble of configurations generated during last 10 iterations of FLC driven WE simulation. The Free energy landscape reconstructed is with respect to  $SI_{noCHOL}$  for DPPC-DAPC-CHOL and DPPC-DIPC-CHOL system respectively. B. The Free energy landscape reconstructed is with respect to  $CEI$  for DPPC-DAPC-CHOL and DPPC-DIPC-CHOL system respectively. The lines are colored to represent different simulation temperatures

landscapes with collective variable candidates that underperformed. Fig 6 A and B show reconstructed free energy landscapes with  $SI_{noCHOL}$  and  $CEI$  by combining the weights from the last ten iterations of four replicas for each system.

The WESTPA framework allows one can resume the WE simulation using variables of choice using the weights from existing ensemble(45, 77). Hence by reusing the unbiased weights on the trajectory ensemble we obtained from a reasonably converged WE simulation, we can rescue the underperformance of WE simulation due to the initial choice of poor collective variable.

### $\Delta\Delta G$ profile of lipid system

From free energy landscapes of lipid bilayer at various temperatures, we can create a  $\Delta\Delta G$  profile by defining an FLC cutoff between mixed and separated states. As seen in Fig 5 A, the concept of state basins is different for a system at different temperatures. In high temperatures, the notion of two states - mixed and separated - breaks down as the double-well behavior of free energy curves turns into a single well. One trivial solution would be to define a rigid FLC cutoff for a system. However, a caveat for this approach, as seen in Fig 5 A, is that the free energy basin for a specific state of the DPPC-DIPC-CHOL system is different for the respective state basin for the DPPC-DAPC-CHOL system. So a rigorous FLC cutoff for the state definition of a system may need to be clarified in another phase-separating system. But to showcase the capability of the pipeline we have

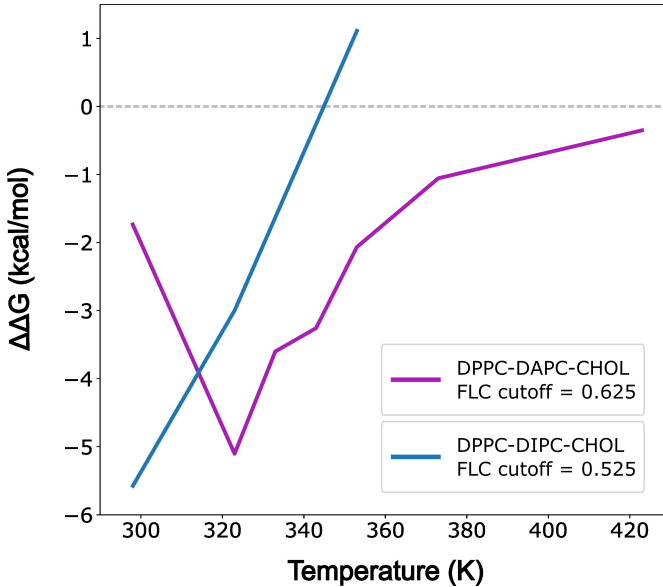


Figure 7:  $\Delta\Delta G$  profile for DPPC-DAPC-CHOL and DPPC-DIPC-CHOL systems for a given cutoff. Each curve represents  $\Delta\Delta G$  for the system to transition from mixed to separated state. Negative values indicate phase coexistence is favored

presented here, we define an ad hoc cutoff,  $FLC = 0.525$  and  $0.625$ , for DPPC-DIPC-CHOL and DPPC-DAPC-CHOL lipid systems respectively. The former means, we make an arbitrary choice of a separated lipid bilayer if more than  $52.5\%$  of lipids in the DPPC-DIPC-CHOL system is part of some clusters. Similarly, the latter implies a higher cutoff for DPPC-DAPC-CHOL system, where more than  $62.5\%$  of lipids are in some clusters. Figure 7 shows the  $\Delta\Delta G$  curve for the DPPC-DAPC-CHOL and DPPC-DIPC-CHOL systems as a function of temperature for respective FLC cutoff. Even though we can see that  $\Delta\Delta G$  curve for mixed to separated transition is crossing  $\Delta\Delta G=0$  line, indicating the corresponding melting temperature, we advise the reader to exercise caution while interpreting this result as we have a coarse-grained model, an arbitrary cutoff, and lack of experimental data to compare it with for given composition. However, we want to highlight the capability of this proof-of-concept pipeline we created to achieve  $\Delta\Delta G$  profiling for a phase-separating system. We expect more accurate profiling by using a more accurate all-atom model for our system with more rigorous methods for defining phase separation in FLC space that account for varying propensity as a function of temperature and system composition. Fig SX shows the sensitivity of FLC cutoffs on  $\Delta\Delta G$  profile for a given system.

## DISCUSSION

### FLOPSS pipeline

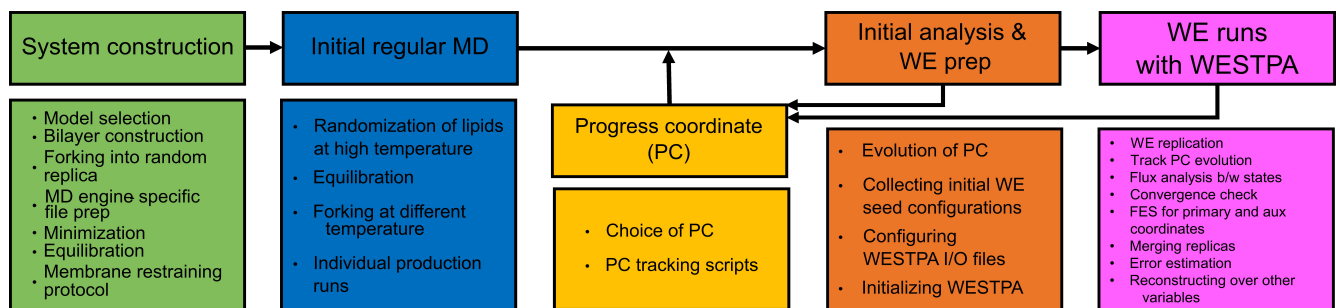


Figure 8: Schematic representation of the proposed FLOPSS pipeline. The pipeline is modular. Each module has layers that can be translated to any phase separating system.

Here we propose a proof-of-concept pipeline to construct **Fre eenergy Landscape Of Phase Separating Systems (FLOPSS)**

by realizing multiple transition events using WE strategy. Even though our systems of interest are lipid bilayers, using appropriate model resolution and collective variables can generalize this pipeline to any system that phase separates. The modular pipeline is outlined in Figure 8, with different sublayers that constitute each module. Given the limitation of the coarse-grained model, free energy landscapes generated by FLOPSS in our positive, test, and negative lipid bilayer system qualitatively agrees with previous literature. For a more quantitative comparison, the next logical step is to use all-atom lipid models. Thus we can investigate both the thermodynamics and kinetics of phase-separating lipid bilayers. Interestingly, many more tools are available from the WE community as the WE strategy has been used predominantly for determining the kinetics of the different systems.

In this work, we have proposed a simple yet efficient collective variable that simultaneously tracks phase separation and drives WE simulation, ensuring sufficient state crossing with reasonable convergence of configurational distribution. We give yet another example of why collective variable choice is crucial for the success of enhanced sampling protocols. The flux analysis presented here only answers how much some proxy labels drive WE simulation better than others. However, our work still needs to explain why that is the case. Thus, a more thorough and systematic analysis of the sensitivity of WE simulation on the choice of collective variable is needed and is unfortunately beyond the scope of this work.

We also acknowledge that certain parameter choices for FLOPSS need further optimization. For example, the current choice of 1 ns as resampling interval,  $\tau$ , for WE simulation is arbitrary. Thus a systematic study of  $\tau$  is needed. Similarly, we have chosen an arbitrary 10-iteration window between successive WEED reweighting to accelerate the convergence. There is room for optimization here as well. Evidence of finite simulation box size effect on domain formations in phase separating lipid bilayer has been reported previously(78). Thus we need to investigate any critical size dependence of free energy landscapes generated by FLOPSS. We acknowledge that the current crude pipeline has scope for further optimization.

In summary, we have developed and validated a new framework that can directly compute the thermodynamics associated with phase separation from simulation. We have also demonstrated the potential reuse of a reasonably converged WE equilibrium simulation driven by a good collective variable to explore other variables which otherwise constitute a poor choice for driving WE simulation. Thus, we can increase the effectiveness of WE simulation without compromising on computational cost. Moreover, we also showcase the potential of FLOPSS to construct a  $\Delta\Delta G$  profile of the system under study to investigate the melting properties.

The FLOPSS pipeline proposed here can be applied to study (a) perturbations in the free energy landscape of lipid bilayer as new species are introduced, such as other lipids, peptides, small molecules, etc. (b) the effects of symmetric and asymmetric bilayer leaflets in phase separation thermodynamics, (c) the differences in free energy landscapes made from CG and all-atom models (d) to derive bilayer properties from an enhanced sampled configurational space than standard MD simulation, etc. Deviating from the lipid bilayer system, we also wish to make FLOPSS more rigorous by testing FLOPSS on toy systems that have simple analytical solutions to compare with. We want to highlight that by generalizing the collective variable FLC to track clustering in 3D space, FLOPSS can also be extended to other instances of biological phase separation. However, this assumes that a reasonable model, forcefield, and computational resources are available to tackle such complex phase-separating systems via MD simulations.

## ACKNOWLEDGEMENTS

The authors thank the Center for Integrated Research Computing (CIRC) at the University of Rochester for providing computational resources and technical support. The authors also thank Prof. Lillian Chong and Prof. Daniel Zuckerman and WESTPA Data and Dev club for insights. The authors thank Anthony Bogetti, Jeremy Leung, John Russo, Dr.Sreyoshi Sur, and Dr.Tod D. Romo for their support. This work was supported by grant R21GM138970 (to A.G.) from the National Institutes of Health.

## REFERENCES

1. Banani, S. F., A. M. Rice, W. B. Peebles, Y. Lin, S. Jain, R. Parker, and M. K. Rosen, 2016. Compositional Control of Phase-Separated Cellular Bodies. *Cell* 166:651–663. <http://dx.doi.org/10.1016/j.cell.2016.06.010>.
2. Banani, S. F., H. O. Lee, A. A. Hyman, and M. K. Rosen, 2017. Biomolecular condensates: Organizers of cellular biochemistry.
3. Larson, A. G., D. Elnatan, M. M. Keenen, M. J. Trnka, J. B. Johnston, A. L. Burlingame, D. A. Agard, S. Redding, and G. J. Narlikar, 2017. Liquid droplet formation by HP1 $\alpha$  suggests a role for phase separation in heterochromatin. *Nature* 547:236–240. <http://dx.doi.org/10.1038/nature22822>.
4. Langdon, E. M., and A. S. Gladfelter, 2018. A New Lens for RNA Localization: Liquid-Liquid Phase Separation. *Annual Review of Microbiology* 72:255–271.

5. Li, P., S. Banjade, H.-c. Cheng, S. Kim, B. Chen, L. Guo, M. Llaguno, J. V. Hollingsworth, D. S. King, S. F. Banani, P. S. Russo, Q.-x. Jiang, B. T. Nixon, and M. K. Rosen, 2012. Phase transitions in the assembly of multivalent signalling proteins. *Nature* 1–6.
6. Sezgin, E., I. Levental, S. Mayor, and C. Eggeling, 2017. The mystery of membrane organization: Composition, regulation and roles of lipid rafts. *Nature Reviews Molecular Cell Biology* 18:361–374. <http://dx.doi.org/10.1038/nrm.2017.16>.
7. Altmeyer, M., K. J. Neelsen, F. Teloni, I. Pozdnyakova, S. Pellegrino, M. Grøfte, M. B. D. Rask, W. Streicher, S. Jungmichel, M. L. Nielsen, and J. Lukas, 2015. Liquid demixing of intrinsically disordered proteins is seeded by poly(ADP-ribose). *Nature Communications* 6.
8. Decker, C. J., and R. Parker, 2012. P-bodies and stress granules: Possible roles in the control of translation and mRNA degradation. *Cold Spring Harbor Perspectives in Biology* 4.
9. Lallemand-Breitenbach, V., and H. de Thé, 2010. PML nuclear bodies. *Cold Spring Harbor perspectives in biology* 2:1–18.
10. Feric, M., N. Vaidya, T. S. Harmon, D. M. Mitrea, L. Zhu, T. M. Richardson, R. W. Kriwacki, R. V. Pappu, and C. P. Brangwynne, 2016. Coexisting Liquid Phases Underlie Nucleolar Subcompartments. *Cell* 165:1686–1697. <http://dx.doi.org/10.1016/j.cell.2016.04.047>.
11. Case, L. B., and C. M. Waterman, 2015. Integration of actin dynamics and cell adhesion by a three-dimensional, mechanosensitive molecular clutch. *Nature Cell Biology* 17:955–963. <http://dx.doi.org/10.1038/ncb3191>.
12. Degreif, D., B. Cucu, I. Budin, G. Thiel, and A. Bertl, 2019. Lipid determinants of endocytosis and exocytosis in budding yeast. *Biochimica et Biophysica Acta - Molecular and Cell Biology of Lipids* 1864:1005–1016. <https://doi.org/10.1016/j.bbaliip.2019.03.007>.
13. Mao, Y. S., B. Zhang, and D. L. Spector, 2011. Biogenesis and function of nuclear bodies. *Trends in Genetics* 27:295–306. <http://dx.doi.org/10.1016/j.tig.2011.05.006>.
14. Boisvert, F. M., S. Van Koningsbruggen, J. Navascués, and A. I. Lamond, 2007. The multifunctional nucleolus. *Nature Reviews Molecular Cell Biology* 8:574–585.
15. Janosi, L., Z. Li, J. F. Hancock, and A. A. Gorfe, 2012. Ras nanoclusters in membrane domains 109.
16. Strulson, C. A., R. C. Molden, C. D. Keating, and P. C. Bevilacqua, 2012. RNA catalysis through compartmentalization. *Nature chemistry* 4:1–6.
17. Li, L., H. Liu, P. Dong, D. Li, W. R. Legant, J. B. Grimm, L. D. Lavis, E. Betzig, R. Tjian, and Z. Liu, 2016. Real-time imaging of Huntingtin aggregates diverting target search and gene transcription. *eLife* 1–29.
18. Jain, A., and R. D. Vale, 2017. RNA phase transitions in repeat expansion disorders. *Nature Publishing Group* 546:243.
19. Ray, S., N. Singh, R. Kumar, K. Patel, S. Pandey, D. Datta, J. Mahato, R. Panigrahi, A. Navalkar, S. Mehra, L. Gadhe, D. Chatterjee, A. S. Sawner, S. Maiti, S. Bhatia, J. A. Gerez, A. Chowdhury, A. Kumar, R. Padinhateeri, R. Riek, G. Krishnamoorthy, and S. K. Maji, 2020.  $\alpha$ -Synuclein aggregation nucleates through liquid–liquid phase separation. *Nature Chemistry* 12:705–716. <http://dx.doi.org/10.1038/s41557-020-0465-9>.
20. Case, L. B., J. A. Ditlev, and M. K. Rosen, 2019. Regulation of Transmembrane Signaling by Phase Separation .
21. Tian, T., A. Harding, K. Inder, S. Plowman, R. G. Parton, and J. F. Hancock, 2007. Plasma membrane nanoswitches generate high-fidelity Ras signal transduction. *Nature Cell Biology* 9.
22. Laganowsky, A., E. Reading, T. M. Allison, M. B. Ulmschneider, M. T. Degiacomi, A. J. Baldwin, and C. V. Robinson, 2014. Membrane proteins bind lipids selectively to modulate their structure and function. *Nature* 510:172–175.
23. Lingwood, D., B. Binnington, T. Rög, I. Vattulainen, M. Grzybek, Ü. Coskun, C. A. Lingwood, and K. Simons, 2011. Cholesterol modulates glycolipid conformation and receptor activity. *Nature Chemical Biology* 7:5–7.
24. Beck-garcía, K., E. Beck-garcía, S. Bohler, C. Zorzin, E. Sezgin, I. Levental, B. Alarcón, and W. W. A. Schamel, 2015. Nanoclusters of the resting T cell antigen receptor ( TCR ) localize to non-raft domains. *Biochimica et Biophysica Acta - Molecular Cell Research* 1853:802–809. <http://dx.doi.org/10.1016/j.bbamcr.2014.12.017>.

25. Wisser, K., M. B. Stone, S. A. Shelby, M. F. Nu, and S. L. Veatch, 2017. Protein sorting by lipid phase-like domains supports emergent signaling function in B lymphocyte plasma membranes. *eLife* 1–33.
26. Dick, R. A., S. L. Goh, G. W. Feigenson, and V. M. Vogt, 2012. HIV-1 Gag protein can sense the cholesterol and acyl chain environment in model membranes. *Proceedings of the National Academy of Science* 109.
27. Klotzsch, E., G. J. Schütz, P. T. R. S. B, and G. J. Schu, 2013. A critical survey of methods to detect plasma membrane rafts A critical survey of methods to detect plasma membrane rafts. *Phil. Trans. R. Soc. B* 368:20120033.
28. Tieleman, D. P., S. J. Marrink, V. Corradi, P. C. T. Souza, H. I. Ingo, M. S. P. Sansom, and A. Tn, 2019. Computational Modeling of Realistic Cell Membranes .
29. Veatch, S. L., S. S. W. Leung, R. E. W. Hancock, and J. L. Thewalt, 2007. Fluorescent Probes Alter Miscibility Phase Boundaries in Ternary Vesicles 502–504.
30. Veatch, S. L., and S. L. Keller, 2003. Letter to the Editor A Closer Look at the Canonical “Raft Mixture” in Model Membrane Studies. *Biophysical Journal* 84:725–726. [http://dx.doi.org/10.1016/S0006-3495\(03\)74891-7](http://dx.doi.org/10.1016/S0006-3495(03)74891-7).
31. Veatch, S. L., and S. L. Keller, 2002. Organization in Lipid Membranes Containing Cholesterol 1–4.
32. Veatch, S. L., and S. L. Keller, 2003. Separation of Liquid Phases in Giant Vesicles of Ternary Mixtures of Phospholipids and Cholesterol. *Biophysical Journal* 85:3074–3083. [http://dx.doi.org/10.1016/S0006-3495\(03\)74726-2](http://dx.doi.org/10.1016/S0006-3495(03)74726-2).
33. Risselad, H. J., and S. J. Marrink, 2008. The molecular face of lipid rafts in model membranes. *Proceedings of the National Academy of Sciences of the United States of America* 105:17367–17372.
34. Lin, X., J. H. Lorent, A. D. Skinkle, K. R. Levental, M. N. Waxham, A. A. Gorfe, and I. Levental, 2016. Domain stability in biomimetic membranes driven by lipid polyunsaturation. *Journal of Physical Chemistry B* 120:11930–11941.
35. Lin, X., and A. A. Gorfe, 2019. Understanding Membrane Domain-Partitioning Thermodynamics of Transmembrane Domains with Potential of Mean Force Calculations. *Journal of Physical Chemistry B* 123:1009–1016.
36. Dror, R. O., R. M. Dirks, J. P. Grossman, H. Xu, and D. E. Shaw, 2012. Biomolecular simulation: A computational microscope for molecular biology. *Annual Review of Biophysics* 41:429–452.
37. Pantelopoulos, G. A., and J. E. Straub, 2018. Regimes of Complex Lipid Bilayer Phases Induced by Cholesterol Concentration in MD Simulation. *Biophysj* 115:2167–2178. <https://doi.org/10.1016/j.bpj.2018.10.011>.
38. Bennett, W. F., J. E. Shea, and D. P. Tieleman, 2018. Phospholipid Chain Interactions with Cholesterol Drive Domain Formation in Lipid Membranes. *Biophysical Journal* 114:2595–2605. <https://doi.org/10.1016/j.bpj.2018.04.022>.
39. Salsburg, Z. W., R. W. Zwanzig, and J. G. Kirkwood, 1953. Molecular Distribution Functions in a One-Dimensional Fluid. *Journal of Chemical Physics* 21:1098–1107.
40. Torrie, G. M Valleau, J., 1977. Nonphysical sampling distributions in Monte Carlo free-energy estimation: Umbrella sampling. *J. Comput. Phys.* 23:187.
41. Hénin, J., T. Lelièvre, M. R. Shirts, O. Valsson, and L. Delemonette, 2022. Enhanced sampling methods for molecular dynamics simulations 4:1–60. <http://arxiv.org/abs/2202.04164>.
42. Fiorin, G., M. L. Klein, and J. Hénin, 2013. Using collective variables to drive molecular dynamics simulations. *Molecular Physics* 111:3345–3362. <http://www.tandfonline.com/doi/abs/10.1080/00268976.2013.813594>.
43. Barducci, A., J. Pfaendtner, and M. Bonomi, 2015. Tackling Sampling Challenges in Biomolecular Simulations. 151–171. [https://link.springer.com/10.1007/978-1-4939-1465-4{\\_}8](https://link.springer.com/10.1007/978-1-4939-1465-4{_}8).
44. Zuckerman, D. M., and L. T. Chong, 2017. Weighted Ensemble Simulation : Review of Methodology , Applications , and Software .

45. Zwier, M. C., J. L. Adelman, J. W. Kaus, A. J. Pratt, K. F. Wong, N. B. Rego, E. Suárez, S. Lettieri, D. W. Wang, M. Grabe, D. M. Zuckerman, and L. T. Chong, 2015. WESTPA: An interoperable, highly scalable software package for weighted ensemble simulation and analysis. *Journal of Chemical Theory and Computation* 11:800–809.
46. Schäfer, L. V., D. H. De Jong, A. Holt, A. J. Rzepiela, A. H. De Vries, B. Poolman, J. A. Killian, and S. J. Marrink, 2011. Lipid packing drives the segregation of transmembrane helices into disordered lipid domains in model membranes. *Proceedings of the National Academy of Sciences of the United States of America* 108:1343–1348.
47. Domański, J., S. J. Marrink, and L. V. Schäfer, 2012. Transmembrane helices can induce domain formation in crowded model membranes. *Biochimica et Biophysica Acta - Biomembranes* 1818:984–994.
48. Jong, D. H. D., C. A. Lopez, and S. J. Marrink, 2013. Molecular view on protein sorting into liquid-ordered membrane domains mediated by gangliosides and lipid anchors † 347–363.
49. Liu, Y., W. Pezeshkian, J. Barnoud, A. H. D. Vries, and S. J. Marrink, 2020. Coupling Coarse-Grained to Fine-Grained Models via Hamiltonian Replica Exchange .
50. Su, J., S. J. Marrink, and M. N. Melo, 2020. Localization Preference of Antimicrobial Peptides on Liquid-Disordered Membrane Domains. *Frontiers in Cell and Developmental Biology* 8:1–11.
51. Davis, R. S., P. B. S. Kumar, M. M. Sperotto, and Laradji Mohamed, 2013. Predictions of Phase Separation in Three-Component Lipid Membranes by the MARTINI Force Field. *Journal of Physical Chemistry B* 117:4072–4080. <https://pubs.acs.org/doi/10.1021/jp4000686>.
52. Qi, Y., H. I. Ingólfsson, X. Cheng, J. Lee, S. J. Marrink, and W. Im, 2015. CHARMM-GUI Martini Maker for Coarse-Grained Simulations with the Martini Force Field. *Journal of Chemical Theory and Computation* 11:4486–4494.
53. Marrink, S. J., H. J. Risselada, S. Yefimov, D. P. Tieleman, and A. H. De Vries, 2007. The MARTINI force field: Coarse grained model for biomolecular simulations. *Journal of Physical Chemistry B* 111:7812–7824.
54. De Jong, D. H., G. Singh, W. F. Bennett, C. Arnarez, T. A. Wassenaar, L. V. Schäfer, X. Periole, D. P. Tieleman, and S. J. Marrink, 2013. Improved parameters for the martini coarse-grained protein force field. *Journal of Chemical Theory and Computation* 9:687–697.
55. Yesylevskyy, S. O., L. V. Schäfer, D. Sengupta, and S. J. Marrink, 2010. Polarizable water model for the coarse-grained MARTINI force field. *PLoS Computational Biology* 6:1–17.
56. Abraham, M. J., T. Murtola, R. Schulz, S. Páll, J. C. Smith, B. Hess, and E. Lindah, 2015. Gromacs: High performance molecular simulations through multi-level parallelism from laptops to supercomputers. *SoftwareX* 1-2:19–25.
57. Bussi, G., D. Donadio, and M. Parrinello, 2007. Canonical sampling through velocity rescaling. *Journal of Chemical Physics* 126.
58. Parrinello, M., and A. Rahman, 1981. Polymorphic transitions in single crystals: A new molecular dynamics method. *Journal of Applied Physics* 52:7182–7190.
59. de Jong, D. H., S. Baoukina, H. I. Ingólfsson, and S. J. Marrink, 2016. Martini straight: Boosting performance using a shorter cutoff and GPUs. *Computer Physics Communications* 199:1–7. <https://linkinghub.elsevier.com/retrieve/pii/S0010465515003628>.
60. Javanainen, M., B. Fabian, and H. Martinez-Seara, 2020. Comment on "Capturing Phase Behavior of Ternary Lipid Mixtures with a Refined Martini Coarse-Grained Force Field" <http://arxiv.org/abs/2009.07767>.
61. Hess, B., H. Bekker, H. J. Berendsen, and J. G. Fraaije, 1997. LINCS: A Linear Constraint Solver for molecular simulations. *Journal of Computational Chemistry* 18:1463–1472.
62. Valsson, O., P. Tiwary, and M. Parrinello, 2016. Enhancing Important Fluctuations: Rare Events and Metadynamics from a Conceptual Viewpoint. *Annual Review of Physical Chemistry* 67:159–184.
63. Yang, Y. I., Q. Shao, J. Zhang, L. Yang, and Y. Q. Gao, 2019. Enhanced sampling in molecular dynamics. *Journal of Chemical Physics* 151. <https://doi.org/10.1063/1.5109531>.

64. Martin Ester, Hans-Peter Kriegel, Jiirg Sander, X. X., 1996. A Density-Based Algorithm for Discovering Clusters in Large Spatial Databases with Noise. *In Proceedings of the 2nd ACM International Conference on Knowledge Discovery and Data Mining (KDD)* 226–231.
65. Schubert, E., J. Sander, M. Ester, H. P. Kriegel, and X. Xu, 2017. DBSCAN revisited, revisited: Why and how you should (still) use DBSCAN. *ACM Transactions on Database Systems* 42. <https://dl.acm.org/doi/10.1145/3068335>.
66. Pedregosa, F. Varoquaux, G. Gramfort, A. Michel, V. Thirion, B. Grisel, O. Blondel, M. Prettenhofer, P. Weiss, R. and Dubourg, V. Vanderplas, J. Passos, A. Cournapeau, D. Brucher, M. Perrot, M. Duchesnay, E., 2011. Scikit-learn: Machine Learning in Python. *Journal of Machine Learning Research* 12:2825—2830.
67. Romo, T. D., N. Leioatts, and A. Grossfield, 2014. Lightweight object oriented structure analysis: tools for building tools to analyze molecular dynamics simulations. *Journal of computational chemistry* 35:2305–2318.
68. Gu, R. X., S. Baoukina, and D. P. Tieleman, 2019. Cholesterol Flip-Flop in Heterogeneous Membranes. *Journal of Chemical Theory and Computation* 15:2064–2070.
69. Gu, R. X., S. Baoukina, and D. Peter Tieleman, 2020. Phase Separation in Atomistic Simulations of Model Membranes. *Journal of the American Chemical Society* 142:2844–2856.
70. Marigo, M., D. L. Cairns, M. Davies, A. Ingram, and E. H. Stitt, 2012. A numerical comparison of mixing efficiencies of solids in a cylindrical vessel subject to a range of motions. *Powder Technology* 217:540–547. <http://dx.doi.org/10.1016/j.powtec.2011.11.016>.
71. Kumar, P., K. Sinha, N. K. Nere, Y. Shin, R. Ho, L. B. Mlinar, and A. Y. Sheikh, 2020. A machine learning framework for computationally expensive transient models. *Scientific Reports* 10:1–11. <https://doi.org/10.1038/s41598-020-67546-w>.
72. Bogetti, A. T., B. Mostofian, A. Dickson, A. Pratt, A. S. Saglam, P. O. Harrison, J. L. Adelman, M. Dudek, P. A. Torrillo, A. J. DeGrave, U. Adhikari, M. C. Zwier, D. M. Zuckerman, and L. T. Chong, 2019. A Suite of Tutorials for the WESTPA Rare-Events Sampling Software [Article v1.0]. *Living Journal of Computational Molecular Science* 1:1–32.
73. Torrillo, P. A., A. T. Bogetti, and L. T. Chong, 2021. A Minimal, Adaptive Binning Scheme for Weighted Ensemble Simulations. *Journal of Physical Chemistry A* .
74. Bhatt, D., B. W. Zhang, and D. M. Zuckerman, 2010. Steady-state simulations using weighted ensemble path sampling. *Journal of Chemical Physics* 133.
75. Suárez, E., S. Lettieri, M. C. Zwier, C. A. Stringer, S. R. Subramanian, L. T. Chong, and D. M. Zuckerman, 2014. Simultaneous computation of dynamical and equilibrium information using a weighted ensemble of trajectories. *Journal of Chemical Theory and Computation* 10:2658–2667.
76. Fowler, P. W., J. J. Williamson, M. S. Sansom, and P. D. Olmsted, 2016. Roles of Interleaflet Coupling and Hydrophobic Mismatch in Lipid Membrane Phase-Separation Kinetics. *Journal of the American Chemical Society* 138:11633–11642.
77. Zhang, B. W., D. Jasnow, and D. M. Zuckerman, 2010. The "weighted ensemble" path sampling method is statistically exact for a broad class of stochastic processes and binning procedures. *Journal of Chemical Physics* 132.
78. Pantelopoulos, G. A., T. Nagai, A. Bandara, A. Panahi, and J. E. Straub, 2017. Critical size dependence of domain formation observed in coarse-grained simulations of bilayers composed of ternary lipid mixtures. *The Journal of Chemical Physics* 147:095101. <http://aip.scitation.org/doi/10.1063/1.4999709>.